AIP | Chaos
An Interdisciplinary Journal of Nonlinear Science
25TH ANNIVERSARY

Nonlinear forecasting of intertidal shoreface evolution

D. J. Grimes, N. Cortale, K. Baker, and D. E. McNamara

Citation: Chaos **25**, 103116 (2015); doi: 10.1063/1.4931801
View online: http://dx.doi.org/10.1063/1.4931801
View Table of Contents: http://scitation.aip.org/content/aip/journal/chaos/25/10?ver=pdfcov
Published by the AIP Publishing

CHAOS 25, 103116 (2015)

Nonlinear forecasting of intertidal shoreface evolution

D. J. Grimes,[1,a)] N. Cortale,[2] K. Baker,[3] and D. E. McNamara[4]
[1]Integrative Oceanography Division, Scripps Institution of Oceanography, University of California San Diego, La Jolla, California 92037, USA
[2]Center for Marine Science, University of North Carolina Wilmington, Wilmington, North Carolina 28409, USA
[3]Geodynamics Group, LLC, Newport, North Carolina 28570, USA
[4]Department of Physics and Physical Oceanography, University of North Carolina Wilmington, Wilmington, North Carolina 28403, USA

(Received 18 June 2015; accepted 14 September 2015; published online 30 September 2015)

Natural systems dominated by sediment transport are notoriously difficult to forecast. This is particularly true along the ocean coastline, a region that draws considerable human attention as economic investment and infrastructure are threatened by both persistent, long-term and acute, event driven processes (i.e., sea level rise and storm damage, respectively). Forecasting the coastline's evolution over intermediate time (daily) and space (tens of meters) scales is hindered by the complexity of sediment transport and hydrodynamics, and limited access to the detailed local forcing that drives fast scale processes. Modern remote sensing systems provide an efficient, economical means to collect data within these regions. A solar-powered digital camera installation is used to capture the coast's evolution, and machine learning algorithms are implemented to extract the shoreline and estimate the daily mean intertidal coastal profile. Methods in nonlinear time series forecasting and genetic programming applied to these data corroborate that coastal morphology at these scales is predominately driven by nonlinear internal dynamics, which partially mask external forcing signatures. Results indicate that these forecasting techniques achieve nontrivial predictive skill for spatiotemporal forecast of the upper coastline profile (as much as 43% of variance in data explained for one day predictions). This analysis provides evidence that societally relevant coastline forecasts can be achieved without knowing the forcing environment or the underlying dynamical equations that govern coastline evolution. © *2015 AIP Publishing LLC*.
[http://dx.doi.org/10.1063/1.4931801]

The evolution of the ocean coastline is important to society as it strongly influences property values and buffers infrastructure from storm damage. Forecasting coastal change is very difficult because underlying grain scale physical processes do not lend themselves to large-scale averaging useful for coastal evolution. In addition, the hydrodynamic forcing directly impacting the region between the ocean and dry sand is complex. We have collected remote camera images of the coastal zone for automated identification of the ocean coastline. We use these images in conjunction with the moving level of the tide to determine the cross-shore shape of the beach at the water's edge. Data measuring this intertidal coastal profile are collected for eight months and used in a nonlinear spatiotemporal series analysis (NSSA) to show that coastal profile evolution is dominated by internal nonlinear dynamics. Methods in nonlinear time series forecasting and genetic programming applied to the data result in nontrivial predictive skill when forecasting daily profile changes. These forecasts provide hope for anticipating coastline change without knowing the complex forcing environment or underlying dynamical equations that govern coastline evolution.

I. INTRODUCTION

The ocean coastline evolves differently at separate spatiotemporal scales: beach cusp patterns occur at spatial scales of centimeters to tens of meters and temporal scales of minutes to days,[15] while cape and spit patterns exist at hundreds of kilometers and evolve over millennia.[2] The two phenomena manifest similar form and rhythmicity, but the dynamics governing these scale-separated features are nonsimilar.[42] Emergence of large-scale coherence and patterning in systems of many interacting constituents is a hallmark of complex systems, in which feedbacks and nonlinear internal dynamics dominate evolution. The extent to which evolution of the intertidal, foreshore profile is controlled by internal nonlinear dynamics, as opposed to responding primarily to the noisy forcing environment, is difficult to quantify. Contemporary models rely heavily on detailed forcing information to make predictions and only weakly account for intrinsic dynamics. The methods here attempt to forecast based solely on previous states without direct knowledge of concurrent forcing. The efficacy of these predictions provides insight about which dynamics dominate evolution at these scales.

Techniques that model the evolution of macroscopic features, like shoreline position or beach profile, using process-based approaches that ramp up granular physics via

[a)]Electronic mail: dgrimes@ucsd.edu

explicit parameterizations (to account for grain size, resuspension/fall rates, and bed friction/percolation, or by way of spatiotemporal patterns in forcing, like edge-waves) are well established. However, these techniques have suboptimal forecast performance and site adaptability when trying to reproduce evolution at a hierarchy of dynamical levels. Alternatively, complexity based approaches attempt to model phenomena using a minimum number of constituents, where fast-scale interactions are connected to the longer time scale dynamics via slaving and self-organization.[42] For example, models simulating the self-organization of beach-cusps capture the spacing and evolution of these features, independently of a matching spatial forcing template.[7,43] Internal nonlinear dynamics have also been shown to influence a system's response to forcing, where behavior may not simply be connected to forcing signatures in time. For example, sediment transport systems can exhibit behavior that masks supply signals within certain ranges of amplitude, outside of which the forcing appears to overbear these dynamics.[19] These examples and others illustrate the importance of nonlinear internal dynamics in contributing to the evolution of natural phenomena without a need for knowledge of fast-time scale dynamics or detailed forcing features.

The relative position of the ocean coastline is an important resource,[18] as it dictates the usable recreational beach and influences property values.[12] Despite its importance to static coastal communities, the region is highly dynamic, varying with tidal elevation, wave set-up, and storm-surge. The magnitude of change in coastline position is regulated by the local slope of the shore-face, the profile of which is not typically linear.[3,8] Characteristics (shape) of the intertidal beach and surf-zone profile are known to adjust in response to changing environmental conditions, and adjustments are not necessarily uniform along the profile.[9,41] Interestingly, despite the myriad of hydrodynamic forcings and sediment compositions, sandy coastlines exhibit a limited range of morphological modes.[25,45]

As a study domain, with the advent of remote imaging systems, the beach is no longer a data poor or expensive subject to research and observe. Comprehensive observations and the development of techniques to extract rigorous, quantifiable features from these sources have led to the development of data driven modeling techniques and forecasting e.g., Refs. 35 and 36. Time series obtained from imaging systems contain information about internal dynamics as they manifest in the system's evolution.[32] According to Takens' Theorem, given sufficient data, a deterministic system's phase space trajectory is reproducible and system evolution may be forecasted.[1,33,40] Specifically, forecasting is based on neighbor trajectories within the embedded phase space, and skill can be affected by the choice of embedding dimension, weighting of neighbor trajectories, the amount of noise in the data, and the prevalence of nonlinear interactions.[34,38]

These nonlinear forecasting techniques have proven capable of outperforming mechanistic models in noisy, nonlinear ecological systems,[29] and they have shown the ability to distinguish noisy natural time series from those governed by nonlinear dynamics.[37] More recently, Genetic Programs have shown the capability of optimizing the search for a global mapping function that projects combinations of lagged values from a time series to future states, with minimal presupposition of their form. This technique has been applied to forecasting of sunspot events, rainfall, and wave heights;[4,23,27] but application to systems that evolve in space and time is lacking. With respect to nonlinear forecasting, this can be thought of as an optimized search for the governing dynamical map that projects a system forward in phase space.

Here, we employ techniques in nonlinear time series analysis and forecasting to explore the extent to which local nonlinear interactions affect day-to-day intertidal profile adjustments. We select shorelines from hourly time lapse images with a four class artificial neural network (ANN).[5,20,31] We compute the mean shoreline position for each image by dividing the area of subaerial beach by the alongshore length of the domain. These measurements in conjunction with near simultaneous tidal elevations and wave data provide daily, two dimensional reconstructions of the foreshore.[30]

A smooth surface is fit to the eight month (8/26/13–4/23/14) time series to filter short lived morphologies,[10] and one day elevation differences are used to lessen the affect of linear autocorrelation.[38] Using a two dimensional extension of nonlinear time series analysis,[28] we attempt to identify whether the system exhibits low-dimensional behavior (nonlinear, chaotic) or stochasticity (linear, noisy) by comparing with synthetic spatiotemporal models in these regimes.[6] We then operate a spatiotemporal genetic program on the intertidal elevation changes to isolate a single mapping of lagged neighbors that achieves the highest predictive skill. The map should converge on the deterministic relationship underlying foreshore dynamics, allowing us to assess the role of both spatial and temporal coupling. We compare these predictions to benchmarks to evaluate forecasting skill.[39]

II. METHODS

The study site is a 300 m alongshore section of south-central Wrightsville Beach, North Carolina. Figure 1 illustrates the location of the camera (red star), the region of interest (yellow boundary), the camera system, and an oblique image from the dataset. The device is located on the roof of a nine-story condominium. Hourly sampling of the region began on August 22, 2013. The data used in this study span to April 23, 2014, at which point the beach underwent an engineered re-nourishment. In conjunction with snapshots, the camera captures a 5 min video and averages the frames to generate a single time lapse image. Image coordinates are converted to physical ground units using an orthorectification procedure.[16,44] The oblique image of Figure 1 is displayed in world coordinates in Figure 2.

The region of interest to society is the subaerial beach. To analyze its behavior, we measured the cross-shore width of the beach in each image. A shoreline detection model was developed using an ANN to isolate the beach from other image components. Time lapse images of the site possess well defined (in color) and fairly homogeneous (in space) regions that coincide with the beach, ocean, vegetation, and

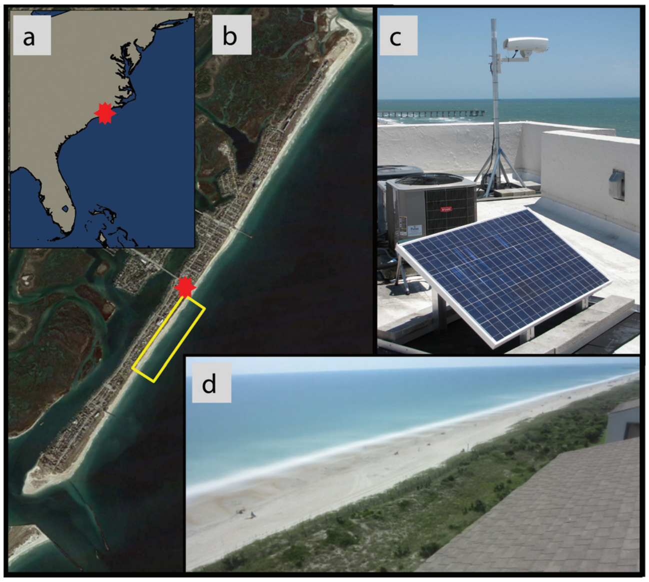

FIG. 1. (a) Eastern seaboard of The United States. The red marker indicates Wrightsville Beach, NC and the camera's location. (b) The yellow rectangle outlines the study region. (c) The remote monitoring camera system. (d) A sample photo obtained from the camera during the survey period.

foam trail from breaking waves. We use the ANN to classify pixel color in red, green, and blue (RGB) space and collapse the 255^3 (8-bit, RGB) possible pixel states to just four. Reference 14 details many classification schemes: ANNs work by inner product activation between vectors in RGB and "neurons" within the networks layers. These pathways are adjusted during training and after which can be applied with consistent precision.[11,13,21]

Several considerations went into the development of the method. First, the selected shoreline should coincide with the seaward edge of the visible beach. It should also provide additional information on the orientation of the beach, such as the dune toe location, or beach curvilinearity and rotation with respect to the geographic coordinates. Hence, a model that also identifies the vegetated region would increase the adaptability of the program to different orientations.

The ANN accomplished these goals, but with some limitations. Manual identification of the visible beach is subjective to the technician because its boundaries are affected by the hydrodynamic conditions, visibility, and image quality. The ANN adopts these intricacies because it is trained on

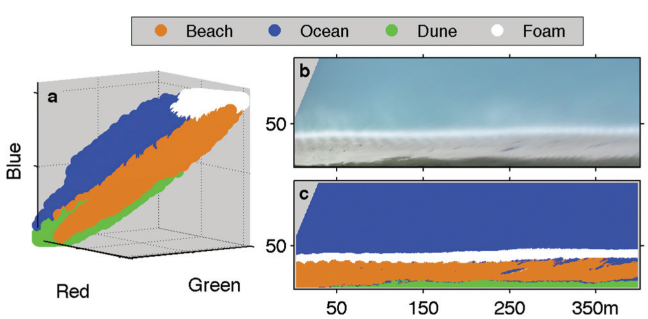

FIG. 2. (a) 3-D axes where RGB vectors from sample images are plotted and colored based on the ANN determined class (see legend). (b) A sample rectified image. (c) The image's classified counterpart.

user selections. Atmospheric conditions also impacted the image's color characteristics. Global color properties were different for images captured on bright versus overcast or dimly lit days. The boundaries between the four RGB domains of Figure 2 were subsequently different under dissimilar conditions. The effect of insolation on image luminosity was managed by concatenating the mean image grayscale value with the RGB vectors fed to the network. In addition, images above (too bright) or below (too dark) a threshold were discarded to further filter the collected data.

Training vectors were manually selected from regions within sufficiently many images to span the range of atmospheric, hydrodynamic, and lighting conditions ($\mathcal{O}(10)$ images were sampled and $\mathcal{O}(10^5)$ pixels were provided to the ANN). The selections were: sandy beach from dune toe to shoreline, ocean (non-wave breaking), foam from wave-breaking, and the vegetative landward area. Matlab routines from the ANN toolbox were used to train a single layer perceptron with 50 neurons and four output classes (one for each aforementioned region). The 3-D axes in Figure 2 illustrate a sampling of the ANN discretized color space. The location of the points corresponds to RGB values and the color signifies the associated classification. The two orthophotos demonstrate an input and classified output image.

In terms of other schemes, it most closely resembles that of Ref. 20, Chap. 4.5, which used a two class ANN with one output to discretize the image domain into subaerial sediment and wetted sand or water; the methods are procedurally distinct, but potentially identify the same "shoreline." The perceptron ANN produces numerical outputs between [0,1], where 0 and 1 may be considered two classification types. A value somewhere between indicates imperfect affiliation with either class type. This information can be used to determine the uncertainty of a given pixel classification, or used for further analysis. In Ref. 20, ANN had three input nodes (the RGB values of a pixel) and one output node. The algorithm used a histogram of the ANN outputs from the entire image to identify the threshold between land and water. The histogram possessed three peaks; at 0 (water), 1 (land), and another somewhere in between that was neither land nor water. The central peak was termed the "shoreline." The peak's proximity to the true waterline varied with wave breaking at the shoreline, run-up characteristics, and/or poor image quality.

Our goal was to consistently identify the visible beach, regardless of the nature of the bordering regions (be it foam, still water, or vegetation). For this reason, we trained an ANN with four output nodes corresponding to the four dominant and distinct color domains in the image (sand, water, foam, and vegetation). The output vector orients the pixel in the 4D classification space, and the index with the largest value was recorded as the identified class. Selection of the shoreline was accomplished in post processing as the seaward edge of the largest contiguous beach region. We stored the pixel length of this shoreward boundary for each measurement and used it for later filtering.

The ANN and feature extraction method identify the division between what the technician identified as subaerial sediment and either foam from swash motions or still water.

It does not locate the instantaneous boundary, because the images are averaged over several minutes. It is likely an underestimate of the physical land-water boundary under low-slope dissipative and outgoing tidal conditions, because seepage from the region upward of the receding waterline can obscure the true position landward. On days with significant activity in the swash zone, the algorithm locates the leading edge of the foam trail; but it is not known how well this corresponds to the maximum run-up achieved during the sampling. It appears consistent in similar conditions.

Image processing provided (u,v) pixel coordinates of the shoreline, which was intersected by two cross-shore boundaries and enclosed by a linear back boundary within the dune. The boundaries were devised relative to the dune-beach boundary and shoreline position in the first image of the record. Determination of the area within this region required constraint of the vertical world coordinate component to the elevation at which the waterline intersected the beach.[16] Estimating this elevation is complicated because discrepancies between measured off-shore and local wave characteristics, and the estimated equilibrium profile and true bathymetry affect induced set-up.[30] Coextensive bathymetric surveys were not available. To limit introduction of further uncertainty and reduce model complexity, the local water elevation, not including tide, was calculated as[24]

$$Z_t = 0.36\beta T_t\sqrt{gH_t}, \tag{1}$$

where g is gravitational acceleration; subscripted t represents time dependent values; T and H are wave period and significant wave height (CDIP buoy no. 150 and 200; NDBC/WMO id. 41110 and 41108), respectively; and β (the slope parameter) was set to the slope of a line fit to the foreshore data from the calmest conditions in the record.[17] This term is an empirical equation for large run-up excursions owing to setup and swash motions and reflects that the shoreline detection algorithm identifies the leading edge of the foam trail left by averaging 5 min of swash motions.

A. Interpolation

The adjusted tidal elevation and alongshore mean shoreline position data posses information on the underlying morphology, as sampled by the waterline. Figure 3 is an example profile from one day of measurement. We assume that the day to day evolution is smooth, and that large or abrupt deviations in the data are an indication of measurement error, or image corruption from environmental conditions (rain, fog, glare, or unaccounted hydrodynamics).

Only shorelines that were confined to the region shoreward of the average breakpoint and seaward of dune toe were processed. Some erroneous classifications persisted and appeared as extremely convoluted, serpentine shorelines. The pixel length of each shoreline identified by image processing was used as a proxy for how well the ANN identified the division between sand and sea. A histogram of these lengths was used to determine acceptable bounds and remove implausible measurements. The choice was made to acknowledged that there was a clear cutoff in the number of pixels that connect the two cross-shore boundaries and that low amplitude rhythmic patterns are prevalent and contribute to a positive skew in the distribution. Measurements of beach width versus tide that were outside of the 95% confidence interval of a least squares regression were also flagged and removed. Errors associated with the shoreline identification and rectification were not quantified.

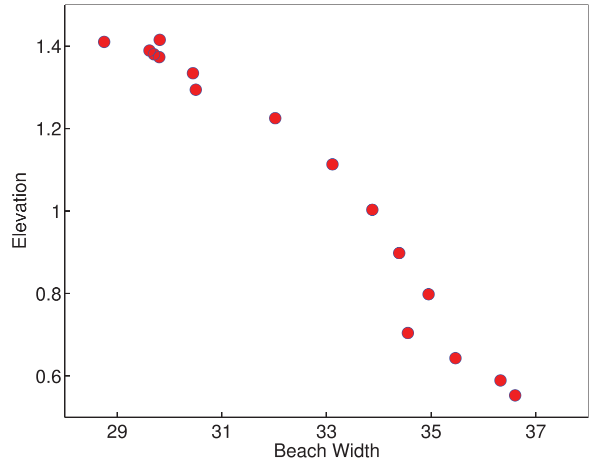

FIG. 3. Water elevation and beach width plotted for one day.

The remaining data, from 6538 images or approximately 70% of the record, were interpolated to a uniformly spaced grid and smoothed to impose continuity.[10] The reconstructed evolution of the intertidal foreshore in Figure 4 was first differenced in time before further analysis. The daily changes in foreshore elevation at each cross-shore cell were compared to daily average wave power (not shown), but no significant correlations were evident.

B. Nonlinear time series analysis

In the one dimensional case, nonlinear time series analysis uses lagged values of a time series to formulate an embedding, which is then analyzed for structure. A reconstruction of the system's state space is performed by generating vectors of the form

$$y_t(x) = (x_t, x_{t-\tau}, \ldots, x_{t-(m-1)\tau}), \tag{2}$$

where x is the time series, subscript t is time, τ is the time lag, y the delay coordinate vector, and m is the dimension of

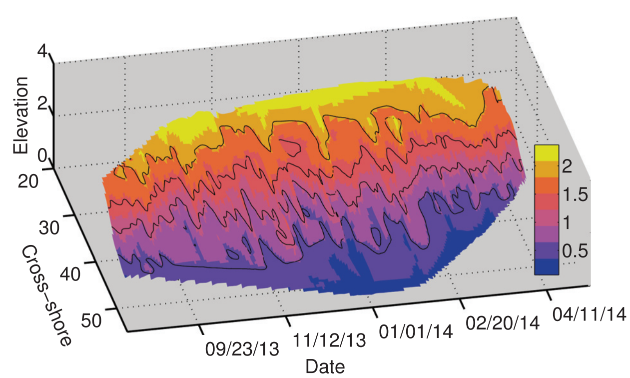

FIG. 4. Reconstructed foreshore time series with level contours at 0.6, 1, 1.4, and 1.8 m.

the reconstructed space. As the dynamical system advances in time, it traces out a trajectory in the reconstructed state space. If the system possesses a smooth attractor, then neighboring trajectories in the space will be well correlated and useful for making predictions of future evolution. These localized properties cause predictive skill to fall as farther trajectories in the space are used to forecast. In this case, the system is characterized by high predictive skill when local trajectories are sampled and lower skill when the range is increased. This behavior is indicative of a system with nonlinear dynamics. Systems without such characteristics—those where predictive skill increases or is unaffected by use of more embedding neighbors—are typically linear. Using this method, nonlinear systems also exhibit prediction-decay, where forecast accuracy falls with increasing prediction step size; linear systems are not similarly affected. Procedurally, one would divide the time series into two components, a sample and testing set: the sample set is used to reconstruct the space and for making predictions on the test set. Performance is calculated over a range of neighborhood and prediction step sizes and provides insight into whether the system is noisy or nonlinear.[6,34,37,38]

Extension of this analysis to multidimensional series, such as those that evolve in space and time, involves the use of lagged and adjacent values from these dimensions to create embedding vectors. For a spatiotemporal series, such as with one spatial and one temporal component, the vectors can be viewed as two dimensional plackets. The essential difference is that y now takes on the form

$$y_{(t,s)}(x) = \left(x_{(t,s)}, x_{(t-\tau,s)}, \ldots, x_{(t-(m-1)\tau, s\pm\frac{n-1}{2}\sigma)}\right), \tag{3}$$

where s refers to the spatial component of the series, σ is the spatial lag, and n is the spatial embedding dimension. The placket is thusly $m \times n$. Near neighbors (NN) in this embedding space are plackets with similar configurations. Lags τ and σ are found from calculating the average mutual information between temporal and spatial sequences of data and lagged versions of such sequences. Once the mutual information is calculated, the first minimum is used as the lag value. The choice of embedding dimension is chosen to maximize predictive skill.

C. Genetic program

The nonlinear time series analysis is a way of distinguishing between nonlinear systems and noisy signals. The method does not provide information on the deterministic relationships underlying the observed behavior, nor is the selected protocol presumed to be the most effective at reproducing system evolution. Floris Takens' delay embedding theorem suggests that there exists a map that projects a deterministic dynamical system forward in time. The procedure used for nonlinear time series analysis is an example of one such mapping, where the map is a function of embedding space neighbors. A map can also relate lagged values of the time series to future states, having the form

$$x_t = \mathcal{F}(x_{t-1}, x_{t-2}, \ldots, x_{t-L}), \quad L+1 \le t \le T. \tag{4}$$

In this representation, $\mathcal{F}$ is some, yet unknown, function of lagged values from the time series, L is the maximum allowable lag, and T is the length of the series.[39]

There are infinitely many possible forms for $\mathcal{F}$, so endeavoring on a global search is intractable. Genetic programs present a means to optimize the search for a governing equation. The principals are rooted in the theories of evolution. The goal is to specialize a set of cursory functions $\{\mathcal{F}_1, \mathcal{F}_2, \ldots\}$ through simulated natural selection, crossover, and mutation. The basic structure of these functions is as follows:

$$\mathcal{F}_i(x) = ((A \otimes B) \otimes (C \otimes D)), \quad 1 \le i \le N, \tag{5}$$

where the letters A, B, C, D refer to either scalar constants, lagged values of the time series (x_{t-l}, $0 \le l \le L$), or entire equation strings. The $\otimes$ can be any of the arithmetic operators, and N is the population size. The set is initialized with randomly selected parameter values, and the probability of $A, \ldots, D$ being either constants or a lagged value of x is predetermined.[39]

The set of equations are used to make predictions on a training section of the dataset, x. Each equation is then ranked based on its fitness, which is computed from

$$R_i^2 = 1 - \frac{SSE_i}{var(x)}, \tag{6}$$

$$r_i^2 = 1 - \left(1 - R_i^2\right)\frac{T_{train} - L - 1}{T_{train} - L - k_i}, \tag{7}$$

where SSE_i is the sum of the squared residuals for the ith equation, $var(x)$ is the variance of the corresponding portion of the time series, T_{train} is the length of the training set, and k_i is the number of variables x_{t-l} used by the ith equation. The fitness (r^2, Eq. (7)) is designed to account for the function's ability to reproduce the variability in the data (R^2, Eq. (6)), and to penalize for length to prevent over-fitting (the k_i term in Eq. (7)).

After ranking, equations with the lowest fitnesses are culled. The remaining equations procreate to generate new equations and refill the empty spots. The reproduction process involves random mutations, in which components are changed with some probability; and includes crossover, where some portion of each parent's equation string is swapped. Over many successive generations the population of equations becomes more specialized at reproducing the behavior of x, and the set converges on the optimal form. At this point, the fittest equation can be tested against an unseen portion of x or used to make forecasts.[39]

D. Synthetic spatiotemporal series

To determine whether the foreshore evolves from nonlinear dynamics, using the nonlinear time series analysis, we needed a basis for comparison. Two synthetic spatiotemporal series were constructed to illustrate the results of performing the intended analysis on a known system from each end of a linear-nonlinear spectrum. A spatiotemporal chaos series was produced from the spatially coupled logistic map

$$x_{t+1} = Ax_t(1 - x_t) \equiv f(x_t), \tag{8}$$

$$x_{t+1,s} = \frac{1}{1+4\epsilon}\left[f(x_{t,s}) + \epsilon f(x_{t,s\pm1}) + \epsilon f(x_{t,s\pm2})\right], \tag{9}$$

where x is the series being generated, A is a constant, f is the logistic function, and ϵ parameterizes the spatial coupling. The other synthetic spatiotemporal series was constructed by adding uncorrelated random noise to a periodic signal in time and space. The test portions of the two synthetics are depicted in Figure 5. The figure also shows the result of adding uncorrelated random noise to the chaotic series and the first difference of Figure 4 taken along the time axis. In adding noise to the chaotic series, we explored a range of added noise levels (from 10% to 80% of the amplitude of the chaotic map) and have chosen to only analyze below the noisy series that most closely matched the analysis on the foreshore data. Each of these four spatiotemporal series will be analyzed using nonlinear time series techniques.

E. Comparative model

Evaluating the quality of these forecasts necessitates a comparative basis. We exploit two heuristic methods, persistence and mean. Persistence forecasts use yesterday's change in beach elevation to estimate, and mean forecasts are made based on the record mean elevation change. We also employ an energy equilibrium model shown in Ref. 46 to capture much of the long time scale (months-years) variability of the mean sea-level contour in response to wave forcing at select sites. The method describes shoreline response based on the dynamical equation

$$\frac{dS}{dt} = C^{\pm}E^{1/2}\Delta E, \tag{10}$$

where $S = S(t)$ is the cross-shore position of the mean water level contour, E is the time dependent wave energy, and $C^{\pm}$ are constants that parameterize the rate of retreat (advance) of the shoreline in response to a positive (negative) energy disequilibrium

$$\Delta E = E - E_{eq}. \tag{11}$$

The equilibrium energy E_{eq} is the energy level for which (10) is zero, and is a linear function of shoreline position

$$E_{eq} = aS + b, \tag{12}$$

where a and b are fit constants.[46] The four model parameters (a, b, and $C^{\pm}$) are optimized through simulated annealing.[22]

To adapt the model to our dataset, we substitute our intertidal foreshore elevation as function of position and time for $S(t)$ (i.e., $S(t) \to S(x,t)$, $\Delta E(t) \to \Delta E(x,t)$). Thus, the model predicts the change in elevation at each cross-shore position in response to forcing. To acknowledge the potential for varying cross-shore dynamics, we allowed the model parameters to vary in x (i.e., $a \to a(x)$, etc.). Our data space has 75 cross-shore cells, giving the model 300 tuning parameters (75 cells $\times$ 4 parameters), which were optimized on the first 2/3 of the dataset.

III. RESULTS

To classify the daily changes in foreshore elevation, we search for analogues between the results of the NSSA applied to the foreshore and surrogate data. We use genetic programming to isolate a deterministic map that describes these dynamics and conduct a rudimentary model comparison with Ref. 46 to provide context for evaluating predictive skill.

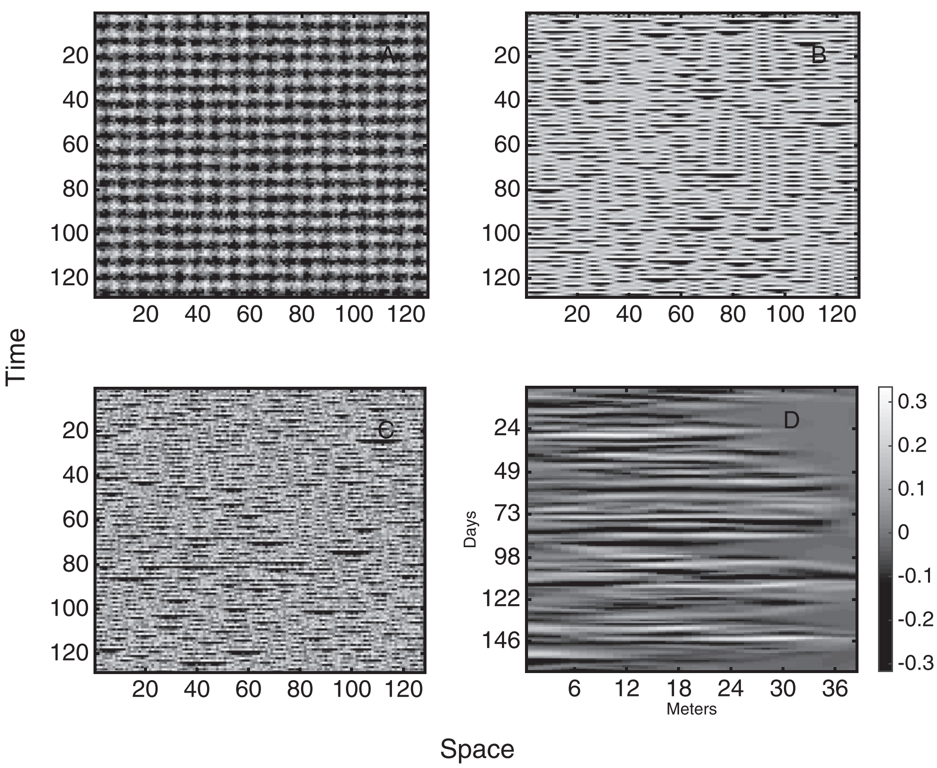

FIG. 5. (a) Uncorrelated random noise added to a linearly periodic function in time and space. (b) Chaotic spatiotemporal series generated with the coupled logistic map. (c) Uncorrelated random noise added to the chaotic spatiotemporal series. (d) The first difference taken along the time axis for the coastal foreshore data.

The domain was split (in time) into a test (last 1/2 of data) and catalogue set (first 1/2). A placket was selected from the test set; matched to a placket (or plackets) with similar structure (NN) in the catalogue set; and the evolution of the NN placket(s) used as a prediction for the test point, which was compared to the actual value. This procedure, when applied to the entire test set, provided statistics on the performance for a given choice of placket size and the number of NN plackets sampled. The placket size was determined by exploring a range of sizes for the determined lags in space and time and choosing the placket with highest predictive skill. The optimal placket size for the foreshore was a three by two placket in space and time ($n = 3$, $m = 2$) where the three space values were lagged five steps apart ($\sigma = 5$) and the two time values were lagged one step in the past ($\tau = 1$). The placket size is analogous to embedding dimension, and the number of NN plackets utilized is similar to the range of embedding space sampled for prediction.[33] The analysis produced the surfaces in Figure 6 where the height of each surface is the RMS error of the prediction divided by the standard deviation of the data. Lower values reflect better predictive skill.

The signature of a nonlinear dynamical system is a prediction skill that peaks at a low-to-intermediate number of near neighbors, and that decreases with forecast step size, and increasing numbers of NN.[37] Figure 6 illustrates these features for the coastline data. For comparison, the same analysis, with appropriate placket adjustments in lag and embedding dimension, was done for the synthetic series. The nonlinear spatiotemporal analysis for the chaotic series with noise added at 50% the amplitude of the signal most closely resembles the results for the coastline foreshore series suggesting that the foreshore is driven by nonlinear dynamics with an overlay of noise. This qualitative similarity with a deterministic nonlinear dynamical system provides a basis for using nonlinear forecasting methods and quantitatively comparing forecasting skill with other methods.

As it appears that the system has localized dynamics in phase space, we can use a genetic program to find the optimum functional relationship between local and past spatiotemporal values in the series. The elevation changes (Figure 5(d)) were fed to a genetic program designed following Ref. 39 and adjusted to include spatial information, which seeks to find a deterministic nonlinear map that projects past spatiotemporal behavior onto future states by optimization of predictive skill.

The population of equations does not have access to the test set (last 1/3 of data) during development. Table I details the results of a run on the foreshore changes in which the maximum allowable temporal lag was set to 20 days and the spatial width set to 5 m. The function uses values in this locale to forecast the future evolution of the point in question. The program trained for 1000 generations, at which point improvements in skill were negligible. The winner

$$x_{(t+1,s)} = \frac{\left(x_{(t,s+1)} + 2x_{(t,s-1)}\right)}{D} - \frac{x_{(t-6,s-1)}}{D^2\left(A + x_{(t-4,s+4)}\right)} - Bx_{(t-1,s-3)} - Cx_{(t-1,s)}, \tag{13}$$

achieved a correlation coefficient of 0.24 when compared to the data for two day predictions; a nontrivial prediction compared to the adapted Ref. 46 model (0.04), persistence (-0.09), in which the forecasted value is that of the day prior, and mean (0.014), which predicts based on the average one day change over the time series. The coefficients $A, \ldots, D$ are $\mathcal{O}(10^{-1} - 10^{0})$ constants whose values are listed in the Appendix. Both presented models outperform Ref. 46

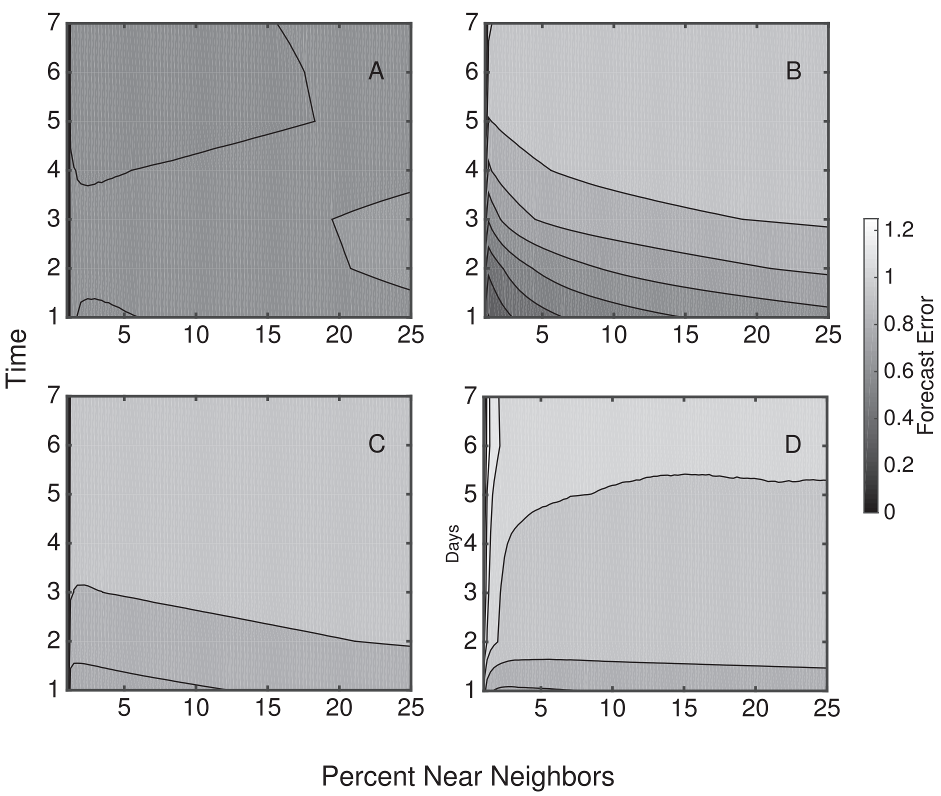

FIG. 6. The RMS forecast error normalized by the standard deviation of the data versus prediction distance in time and number of near neighbors used to generate the prediction for (a) uncorrelated random noise added to a periodic function, (b) chaotic spatiotemporal series, (c) chaotic spatiotemporal series with noise added, and (d) first difference in time axis for the coastal foreshore data.

TABLE I. Comparison of results from the genetic program's (Gen. Pgm.) winning equation to the nonlinear spatiotemporal series analysis (NSSA) and to benchmarks.

Prediction step	Gen. Pgm.	NSSA	Yates	Persistence	Mean
1 day	0.64	0.63	0.015	0.49	0.014
2	0.24	0.30	0.04	−0.09	…
4	0.16	0.25	0.09	−0.14	…
7	0.11	0.03	0.05	−0.06	…

model for prediction horizons ≤ 6 days, while the genetic program's equation manages to overtop the benchmarks out to 10 day forecasts.

A. Discussion

The methods and results presented suggest the coastal intertidal foreshore is strongly influenced by nonlinear spatiotemporal dynamics. This validates the use of nonlinear modeling in simulating coastal dynamics, but points to a deficiency in weakly nonlinear models, that local sediment exchanges appear to overbear the forcing signal at the present scale.

Limitations of the analysis include inherent uncertainties in the image processing and shoreline extraction methods. The shoreline extracted by the presented method is comparable to manual identification; however, unlike manual selection, which is subjective, the algorithm will choose the same shoreline when presented the same image twice. To its detriment, it could not differentiate images where the shoreline was obscured, and thusly required filtering. Adjustments for wave runup were hampered by the fact that local wave information from the Masonboro Inlet buoy (CDIP no. 150) was unavailable for 60% of the survey period and hence the next nearest buoy in the region was utilized (Wilmington Harbor buoy CDIP no. 200). The noise introduced to the data via shoreline misidentification and elevation error are partially visible in the scatter of Figure 3 about the underlying profile. However, despite these avenues for noise in the dataset, the model-free nonlinear methods performed well.

We suspect Ref. 46 model was negatively affected by the proxy wave data, as the model depends on precise forcing information. The mapping function in Equation (10) also suggests that the poor performance may be attributable to unaccounted spatial sediment exchanges that occur along the profile as that map bases predictions on a weighted sum of previous adjacent neighbor changes (1st, 3rd, and 4th term RHS). It also exhibits some longer time scale memory, using a lagged neighbor from 6 days prior (2nd term RHS). The lagged spatial terms in the mapping function suggest that planform coastline evolution on daily time scales is strongly influenced by sediment exchanges in the intertidal profile. This suggests that coastline models that do not include these dynamics will perform poorly in forecasting daily coastline behavior.

IV. CONCLUSIONS

Collection of remote images of the nearshore region and classification using a newly extended neural network procedure has provided a series of spatiotemporal images of the upper shore-face. High predictive skill from the novel application of both spatiotemporal nonlinear time series forecasting and a spatiotemporal map function found using genetic programming suggest that the evolution of this coastal morphology is governed by nonlinear dynamics. Both prediction techniques outperformed persistence predictions over many days and therefore provided useful advances in forecasting the evolution of the coastline.

A number of numerical models exist that attempt to simulate the dynamics of shore face evolution[47] but the efficacy of model predictions is limited (Table I),[26] and in all cases models require local external forcing conditions for model dynamics and fitting of model free parameters to historical data. The forecasting techniques used here yield useful forecasts without the need for tuning parameters in dynamical equations or detailed local hydrodynamic conditions which can often be difficult to ascertain in advance, particularly within the surf zone. The methods used here do require choices for parameter values but some values, such as lags in the nonlinear forecasting technique, can be determined according to explicit tests that are not based on data fitting. Other parameters, mutation and crossover rate in the genetic programming method for example, are not amenable to explicit tests but unlike fast-scale dynamical shoreline models, the number of parameters is small and results are insensitive to a range of values.

With significant human enterprise located in coastal regions around the world, there is a high premium placed on the ability to predict coastline behavior. Our results suggest that remote observations and nonlinear prediction techniques applied to collected observations should be pursued in concert with continued investigations into the underlying dynamical equations for morphological evolution.[47]

ACKNOWLEDGMENTS

The authors thank Mark Lammers, Kenneth Ells, and reviewers for helpful comments to improve the manuscript. Support for this project was provided by UNCW and the National Science Foundation (EAR-1053113).

APPENDIX: GENETIC PROGRAM CONSTANTS

$$A = 0.816986456653888$$
$$B = 0.163755957814937$$
$$C = 0.374463836371727$$
$$D = 3.610369962119076$$

[1]Abarbanel, H. D. I., *Analysis of Observed Chaotic Data* (Springer, 1997).
[2]Ashton, A. A., Murray, B., and Arnault, O., "Formation of coastline features by large-scale instabilities induced by high-angle waves," Nature **414**, 296–300 (2001).
[3]Aubrey, D. G., Inman, D. L., and Nordstrom, C. E., "Beach profiles at Torrey Pines, CA," in *Proceedings of the Fifthteenth International Conference on Coastal Engineering* (American Society of Civil Engineers, 1977), pp. 1297–1311.
[4]Basu, S., Sarkar, A., Satheesan, K., and Kishtawal, C. M., "Predicting wave heights in the North Indian ocean using genetic algorithm," Geophys. Res. Lett. **32**, 4232–4244 (2005).
[5]Boak, E. H. and Turner, I. L., "Shoreline definition and detection: A review," J. Coastal Res. **21**, 688–703 (2005).

[6]Casdagli, M., "Chaos and deterministic versus stochastic non-linear modelling," J. R. Stat. Soc., Ser. B (Methodological) **54**, 303–328 (1992).
[7]Coco, G., Burnet, T. K., Werner, B. T., and Elgar, S., "Test of self-organization in beach cusp formation," J. Geophys. Res. **108**, 3101, doi:10.1029/2002JC001496 (2003).
[8]Dean, R. G., *Equilibrium Beach Profiles: U.S. Atlantic and Gulf Coasts* (Department of Civil Engineering, Ocean Engineering Report No. 12, University of Delaware, Newark, Delaware, 1977).
[9]Dean, R. G., "Equilibrium beach profiles: Characteristics and applications," J. Coastal Res. **7**, 53–84 (1991).
[10]Garcia, D., "Robust smoothing of gridded data in one and higher dimensions with missing values," Comput. Stat. Data Anal. **54**, 1167–1178 (2010).
[11]Gardner, M. W. and Dorling, S. R., "Artificial neural networks (the multilayer perceptron)—A review of applications in the atmospheric sciences," Atmos. Environ. **32**, 2627–2636 (1998).
[12]Gopalakrishnan, S., Smith, M., Slott, J., and Murray, B., "The value of disappearing beaches: A hedonic pricing model with endogenous beach width," J. Environ. Econ. Manage. **61**, 297–310 (2011).
[13]Hagan, M. T., Demuth, H. B., and Beale, M., *Neural Network Design* (PWS Publishing Company, Boston, MA, 1996).
[14]Hastie, T., Tibshirani, R., and Friedman, J., *The Elements of Statistical Learning: Data Mining, Inference and Prediction*, 2nd ed., Springer Series in Statistics (Springer, 2009).
[15]Holland, T. K., "Beach cusp formation and spacing at duck, USA," Cont. Shelf Res. **18**, 1081–1098 (1998).
[16]Holland, T. K., Holman, R. A., Lippmann, T. C., Stanley, J., and Plant, N., "Practical use of video imagery in nearshore oceanographic field studies," IEEE J. Oceanic Eng. **22**, 81–92 (1997).
[17]Holman, R. A. and Sallenger, A. H., Jr., "Setup and swash on a natural beach," J. Geophys. Res. **90**, 945–953, doi:10.1029/JC090iC01p00945 (1985).
[18]Houston, J. R., "The economic value of beaches—A 2013 update," Shore Beach **81**, 3–11 (2013).
[19]Jerolmack, D. J. and Paola, C., "Shredding of environmental signals by sediment transport," Geophys. Res. Lett. **37**, L19401, doi:10.1029/2010GL044638 (2010).
[20]Kingston, K. S., "Applications of complex adaptive systems approaches to coastal systems," Ph.D. dissertation (University of Plymouth, 2003).
[21]Kingston, K. S., Ruessink, B. G., van Enckevort, I. M. J., and Davidson M. A., "Artificial neural network correction of remotely sensed sandbar location," Mar. Geol. **169**, 137–160 (2000).
[22]Kirkpatrick, S., Gelatt, C. B., and Vecchi, M. G., "Optimization by simulated annealing," Science **220**, 671–680 (1983).
[23]Kishtawal, C. M., Basu, S., Patadia, F., and Thapliyal, P. K., "Forecasting summer rainfall over india using genetic algorithm," Geophys. Res. Lett. **30**, 2203, doi:10.1029/2003GL018504 (2003).
[24]Komar, P. D., *Beach Processes and Sedimentation* (Prentice Hall Inc., Upper Saddle River, New Jersey, 1998), p. 544.
[25]Lippmann, T. C. and Holman, R. A., "The spatial and temporal variability of sand bar morphology," J. Geophys. Res. **95**, 11575–11590, doi:10.1029/JC095iC07p11575 (1990).
[26]Madsen, A. J. and Plant, N. G., "Intertidal beach slope predictions compared to field data," Mar. Geol. **173**, 121–139 (2001).
[27]Orfila, A., Ballester, J. L., Oliver, R., Alvarez, A., and Tintore, J., "Forecasting the solar cycle with genetic algorithms," Astron. Astrophys. **386**, 313–318 (2002).
[28]Parlitz, U. and Merkwirth, C., "Prediction of spatiotemporal time series based on reconstructed local states," Phys. Rev. Lett. **84**, 1890–1893 (2000).
[29]Perretti, C. T., Munch, S. B., and Sugihara, G., "Model-free forecasting outperforms the correct mechanistic model for simulated and experimental data," Proc. Natl. Acad. Sci. U. S. A. **110**, 5253–5257 (2013).
[30]Plant, N. and Holman, R., "Intertidal beach profile estimation using video images," Mar. Geol. **140**, 1–24 (1997).
[31]Plant, N. G., Aarninkhof, S. G. J., Turner, I. L., and Kingston, K. S., "The performance of shoreline detection models applied to video imagery," J. Coastal Res. **23**, 658–670 (2007).
[32]Plant, N. G., Holland, T. K., and Holman, R. A., "A dynamical attractor governs beach response to storms," Geophys. Res. Lett. **33**, L17607, doi:10.1029/2006GL027105 (2006).
[33]Rubin, D. M., "Use of forecasting signatures to help distinguish periodicity, randomness, and chaos in ripples and other spatial patterns," Chaos **2**, 525–535 (1992).
[34]Sauer, T., Yorke, J. A., and Casdagli, M., "Embedology," J. Stat. Phys. **65**, 579–616 (1991).
[35]Smit, M. W. J., Aarninkhof, S. G. J., Wijnberg, K. M., Gonzalez, M., Kingston, K. S., Southgate, H. N., Ruessink, B. G., Holman, R. A., Siegle, E., Davidson, M., and Medina, R., "The role of video imagery in predicting daily to monthly coastal evolution," J. Coastal Res. **54**, 539–553 (2007).
[36]Smith, R. K. and Bryan, K. R., "Monitoring beach face volume with a combination of intermittent profiling and video imagery," J. Coastal Res. **23**, 892–898 (2007).
[37]Sugihara, G., "Nonlinear forecasting for the classification of natural time series," Philos. Trans.: Phys. Sci. Eng. Chaos Forecasting **348**, 477–495 (1994).
[38]Sugihara, G. and May, R. M., "Nonlinear forecasting as a way of distinguishing chaos from measurement error in time series," Nature **344**, 734–741 (1990).
[39]Szpiro, G. G., "Forecasting chaotic time series with genetic algorithms," Phys. Rev. E **55**, 2557–2568 (1997).
[40]Takens, F., "Detecting strange attractors in turbulence," *Dynamical Systems and Turbulence, Warwick 1980* (Springer Berlin Heidelberg, 1981), pp. 366–381.
[41]Thom, B. G. and Hall, W., "Behavior of beach profiles during accretion and erosion dominated periods," Earth Surf. Processes Landforms **16**, 113–127 (1991).
[42]Werner, B. T., "Complexity in natural landform patterns," Science **284**, 102–104 (1999).
[43]Werner, B. T. and Fink, T. M., "Beach cusps as self-organized patterns," Science **260**, 968–971 (1993).
[44]Wolf, P. R., *Elements of Photogrammetry with Air Photo Interpretation and Remote Sensing* (McGraw Book Co., 1974), pp. Appendices A–C.
[45]Wright, L. D. and Short, A. D., "Morphodynamic variability of surf zones and beaches: A synthesis," Mar. Geol. **56**, 93–118 (1984).
[46]Yates, M. L., Guza, R. T., and O'Reilly, W. C., "Equilibrium shoreline response: Observations and modeling," J. Geophys. Res. **114**, C09014, doi:10.1029/2009JC005359 (2009).
[47]Yates, M. L., Guza, R. T., O'Reilly, W. C., Hansen, J. E., and Barnard, P. L., "Equilibrium shoreline response of a high wave energy beach," J. Geophys. Res. **116**, C04014, doi:10.1029/2010JC006681 (2011).